

Computer vision for focus calibration of photo-polymerization systems

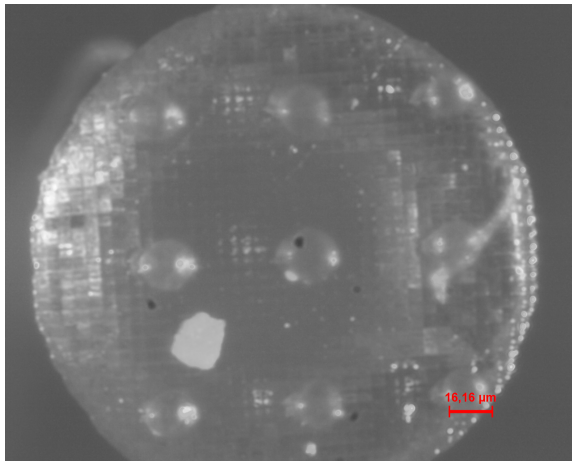
Christian K. Ingwersen¹, Harald L. Mortensen¹, Macarena M. Ribo², Anna H. Danielak², Eythor R. Eiriksson¹, Allan A. Nielsen¹ and David B. Pedersen²

¹Dept. of Applied Mathematics and Computer Science, Technical University of Denmark, Kgs. Lyngby, Denmark

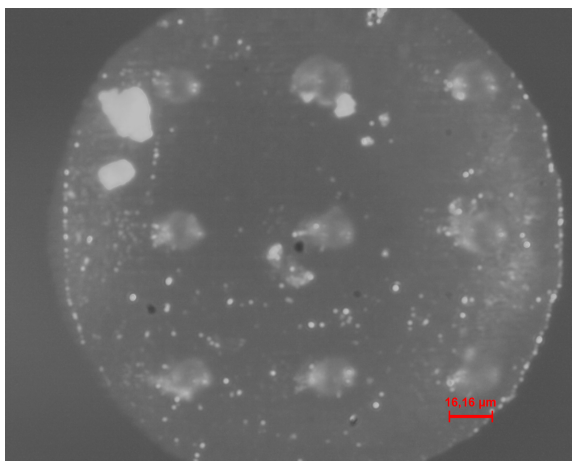
²Dept. of Mechanical Engineering, Technical University of Denmark, Kgs. Lyngby, Denmark

INTRODUCTION

Photopolymerization by mask projection allows for rapid construction of extremely detailed and intricate objects, such as hearing aids. The Technical University of Denmark has long had an interest in applying computer vision to additive manufacturing systems in order to increase printing quality. To obtain the optimal printing quality for photopolymerization systems, it is paramount that the focal plane is exactly at the build plane. Manually finding the position of optimal focus is an arduous and time-consuming task. Previous attempts at implementing an automatic procedure for finding the optimum focus has failed [1].



((a)) In focus



((b)) Out of focus

Figure 1: Effect on print precision when the printer is in focus compared to slightly out of focus. For the in focus print, the projection from each single micromirror can clearly be distinguished. This is not the case for the out of focus print. As such, out of focus prints have much lower precision.

In this paper we present an autofocus solution for mask projection based photopolymerisation systems (MPPSs), with ease-of-use equivalent to the autofocus known from an ordinary DSLR-camera. The autofocus solution has been implemented and tested on the experimental MPPS (Figure 2) at Technical University of Denmark, Department of Mechanical Engineering using a PointGrey Blackfly S BFS-U3-51S5M-C industrial CCD-camera, no lens and a pixel size of $3.45\mu\text{m}$. The MPPS is built using a Visitech Luxbeam Rapid System projector of LRS-WQ-HY, with a micromirror size of $7.5\mu\text{m}$ and depth of focus range of $\pm 50\mu\text{m}$ for the 1.0 magnification filter and $\pm 200\mu\text{m}$ for the 2.0 magnification filter [2], [3]. The lateral movement of the projector is built with a motorized projector mount with a minimum step size of $1.56\mu\text{m}$. By projecting a checkerboard pattern from the projector up onto the glass plate where the camera is mounted and moving the projector laterally, we are able to implement autofocus.

In Figure 1, two different prints from on the experimental printer in Figure 2 can be seen. In the top print we can see the projection of each of the small micromirrors and every intricate detail in the print. For comparison, in the bottom out of focus print, none of these details can be seen and it is impossible to discern the projection from each micromirror.

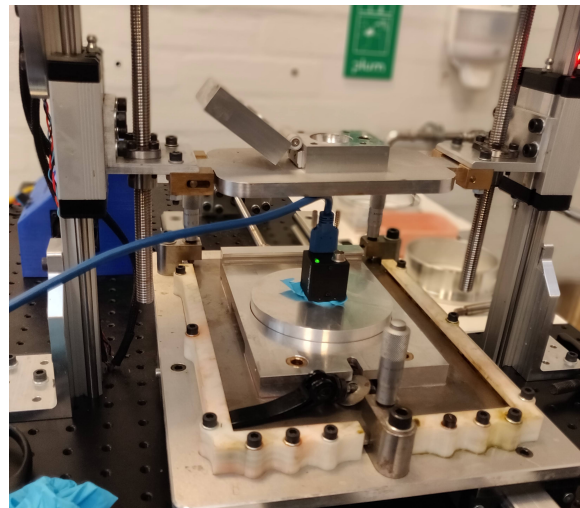


Figure 2: The mask projection based photopolymerisation system at DTU Dept. of Mechanical Engineering. The autofocus is performed by placing the Blackfly S camera in a mount atop the glass-bottom of the vat.

Our autofocus solution allows researchers faster and easier access to building on the MPPS, requiring no training in using calibration software or printer operating procedure outside the standard.

EVALUTING FOCUS

The autofocus algorithm is built using a multi-scale global search algorithm with a local curve fitting approach based on a carefully chosen focus-measure. The choice of focus measure is the essence of the autofocus solution and is indeed a non-trivial issue. For humans it is easy to see whether or not the patterns in Figure 3 are in focus or out of focus, but no general measure of the degree of focus exists.

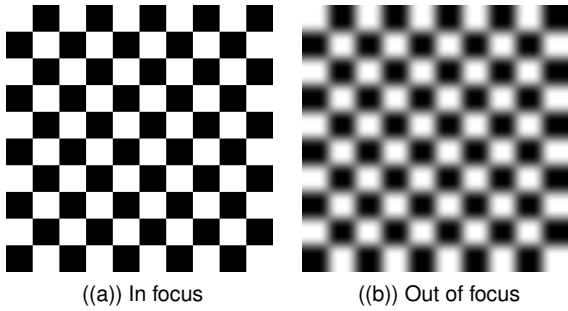


Figure 3: Visualization of in focus and out of focus checkerboard pattern.

Investigating Figure 3, it can be seen that as an image is defocused, sharp features are decreased and small details disappear. This defocus is observable as a blurring and a decrease in contrast, hence we assume that an image with a great amount of high frequency features will be in focus. As such, we propose a focus measure based on the sum of the Discrete Fourier Transform,

$$f^{SDFT} = \sum_{m=1}^M \sum_{n=1}^N |DFT(I)(m,n)|. \quad (1)$$

By the nature of images as inherently discrete collections of information, it would be interesting to consider another transform instead based on functions with finite support. An example of this is the Haar transform, which we have used to construct a focus measure as the weighted sum of Haar components,

$$F_{ab}^{Haar,s,2^n} = \sum_{i=1}^N \sum_{j=1}^M \left[a |\mathcal{V}_s(i,j)| + b |\mathcal{H}_s(i,j)| \right]^n, \quad (2)$$

where \mathcal{V}_s , \mathcal{H}_s are resp. the vertical and horizontal differences from s iterations of the Haar-transform and N, M are the dimensions of each resulting component.

In Figure 3 it is seen that blurring is especially apparent in regards to edges, as these shift from being high gradient areas to low gradient areas. As such, in establishing a measure to evaluate the level of focus in images, it is reasonable to expect measures dealing with the gradients of images to do well in detecting focus. We present the sum of the absolute gradients as

a focus measure,

$$f^{ATG} = \sum_{m=1}^M \sum_{n=1}^N |\nabla I(m,n)|, \quad |\nabla| = \left| \frac{\partial I}{\partial x} \right| + \left| \frac{\partial I}{\partial y} \right|. \quad (3)$$

The Laplacian of an image is a measure of how fast the intensity changes. For a defocused image, edges are blurred, causing the change in gradients to decrease. The variance of Laplacian would then be a quantification of the number and magnitude of sharp edges. As such, we introduce the variance of the Laplacian as a focus measure,

$$f^{VIL} = \mathbb{V} [|\nabla^2 I(m,n)|], \quad |\nabla^2| = \left| \frac{\partial^2 I}{\partial x^2} \right| + \left| \frac{\partial^2 I}{\partial y^2} \right|. \quad (4)$$

In literature several other focus measures have been proposed and we refer the reader to [4] and [5], for an in depth study of focus measure selection. In order to decide on an optimal focus measure for our specific autofocus solution on the experimental MPPS, we have captured a dataset. The dataset consists of 200 images evenly captured over a range of $3.3mm$, with the optimal focus approximately near the center of the dataset. To validate the focus measures, each of them are evaluated on the dataset and the resulting graphs can be seen in Figure 4.

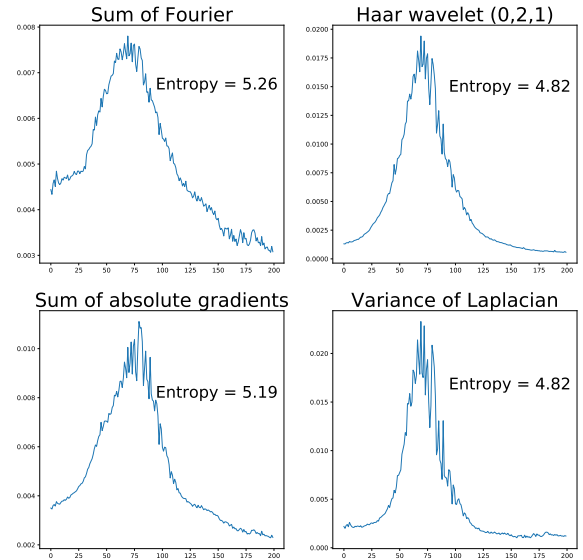


Figure 4: The four focus measures presented in Equation (1-4) evaluated on the dataset of 200 images captured around the manually found optimal focus. Each of the focus measure graphs are normalized to have an area of 1.

From Figure 4 it can be seen that all of the four proposed focus measures fortunately have an approximately unimodal graph when evaluated on the 200 images. A good focus measure is a measure in which the peak is clearly pronounced, but since all of the proposed focus measures are fairly well-behaved, we require some quantitative method to choose the best measure. To accomplish this, we have performed a multivariate analysis using PCA to maximize variance along the y-axis. We find that all of our measures are

approximately unimodal and all are in general consensus of where the optimal focus is found. As such, the variance of each measure largely stems from the peak. Therefore, the multivariate measure which maximizes variance will also contain a clear peak. The loadings of this multivariate measure then signify which focus measure contributes the most to this y -axis variance - and thus to the peak. The measures with highest loadings will then be the measures which best describe the structure of the multivariate measure. As such, we can use these loadings as a ranking of focus measures, where higher loadings translate to better measures. The loadings L are illustrated in Equation 5, ordered as: Sum of Fourier, Haar wavelet, Sum of Absolute Gradients, Variance of Laplacian.

$$L = [0.162 \quad 0.649 \quad 0.286 \quad 0.686]. \quad (5)$$

Thus, we find that the Haar wavelet and Variance of Laplacian focus measures explain the most variance, which indicates that they are better measures.

However, calculating which focus measure explains the most variance in our data is not sufficient in determining which focus measure actually performs best. If a measure varies wildly but has no definitive peak, it has a large variance but is not at all suitable for finding a good focus. As such, we would also like to quantify the "peakedness" of each measure using the Shannon Entropy, Equation 7.

For a Gaussian distribution with large variance in the x -direction, i.e. a less-defined peak, the entropy will also be large. A small variance in the x -direction will result in a clearer peak and low entropy. As we wish for our focus measures to exhibit "peakedness", we would thus like for them to have low entropy. As such, we can use entropy as a criterion for evaluating focus measures. For K positions of a camera in relation to an object, we can evaluate each of our four different focus measures. We will thus define an observation of a focus measure $s \in \{1, \dots, S\}$ evaluated at image $k \in \{1, \dots, K\}$ as $FM_s(k)$. If we wish to view our observations of focus measures as discrete probability distributions, we can define each distribution P_s as,

$$P_s(k) = \frac{FM_s(k)}{\sum_{k=1}^K FM_s(k)}, \quad s \in \{1, \dots, S\}, k \in \{1, \dots, K\}, \quad (6)$$

thus satisfying that $\sum_{k=1}^K P_s(k) = 1, s \in \{1, \dots, S\}$. By doing this, we can calculate the Shannon Entropy for each of our focus measures as,

$$H_s = - \sum_{i=1}^K P_s(k_i) \log(P_s(k_i)), \quad (7)$$

yielding the Entropy as illustrated in Figure 4. By inspecting these, we see that the Haar and Laplacian based focus measure are equal in "peakedness". However, from principal component analysis we found that the Variance of Laplacian measure had a higher loading than the Haar measure, thus indicating

that it must be a slightly better measure. Based on our investigation we conclude that the Variance of Laplacian presented in Equation 4 is the most suited focus measure for our MPPS autofocus solution.

SEARCHING SMART

The search section of the auto-focus algorithm is a multi-scale global search combined with curve fitting, as presented in [6]. This algorithm requires a starting and end point of our search-interval, an initial step-size and a desired threshold defining how accurate we want our result from the search to be.

One could choose to use the entire accessible range of $325mm$ as the initial search interval with a coarse step-size, but the range in which the CCD can capture actual data and not just noise is only about $10mm$ wide. Starting our algorithm on the entire range with too coarse a step size would, in worst-case scenario, result in not capturing any data in the usable range and hence the algorithm would only be dealing with input that is almost purely noise. Therefore we recommend that the initial search range is set to the interval in which some parts of the pattern is actually visible, along with a step-size at around $1mm$.

The starting position is denoted $R_0^t \geq 0$, the end position R_n^t , assuming $R_0^t < R_n^t, \forall t$ and the initial step-size S_0 . A number of images in the initial search interval are acquired, the focus measure at each step is evaluated and the position of the maximum focus in the interval is denoted FM_{max}^t .

Next the distances from FM_{max}^t to R_0^t and R_n^t are found and the maximum distance is denoted D_t , i.e. $D_t = \max(|FM_{max}^t - R_0^t|, |FM_{max}^t - R_n^t|)$. The maximum distance, D_t is used to update the search interval and step-size. The new range is updated by $R_0^{t+1} = FM_{max}^t - \frac{D_t}{2}$, $R_n^{t+1} = FM_{max}^t + \frac{D_t}{2}$. The updated step-size is $S_{t+1} = \frac{D_t}{D_{t-1}} S_t$.

This is repeated until the distance between the current optimal focus position and the one in the previous step goes below a certain threshold. To minimize noise and improve accuracy, the maximum of a second order polynomial fitted to the data at a small range around the found optimal position, is chosen as the optimal focus.

This approach allows us to achieve high accuracy quickly. As an alternative we could use a global search over the visible range at the minimum step size at $1.56\mu m$, however this would require around $10/0.00156 \approx 6400$ steps. Assuming each step takes around 1 second, this would take more than a 100 minutes. For comparison our solution with the proposed algorithm takes approximately 4 minutes to find the position of the optimal focus.

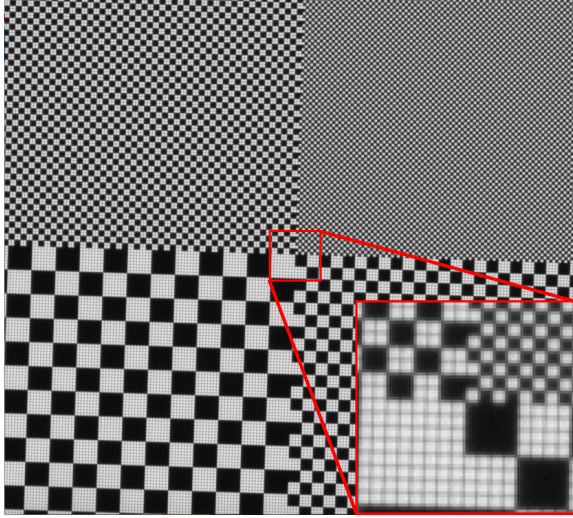


Figure 5: An in-focus view of the checkerboard calibration-mesh taken at the detected point of optimal focus, corresponding to the peak of Variance of Laplacian in Figure 4. Each tiny square in the top right corner is the projection from one micromirror.

VALIDATION

A challenge in the implementation of an autofocus solution for a mask projection based photopolymerization system, is the fact that the depth of focus of these projectors is generally very low, especially when equipped with the short focal length 1.0-magnification lenses. Once we are out of the depth of focus, the noise level increases drastically, until there is no discernible signal left. As such, if the initial sweep is performed such that it misses the narrow band of actual signal, it breaks down completely. We propose two solutions for this problem, dependent on whether there is prior knowledge of where the in-focus position is. If no prior knowledge, a much more fine-grained sweep is needed. If prior knowledge, then only a small area around the presumed in-focus position is searched.

In validating whether the found optimal point of focus is actually the optimum, we need to inspect the calibration mesh as it appears at this position. By using a checkerboard calibration-mesh with the same resolution as the MPPS, determining the degree of focus corresponds to evaluating how discernible each micromirror is from each other. In Figure 5 each micromirror can clearly be distinguished, thus making it clear that this position is in fact very much in-focus.

RESULTS

By using the Variance of Laplacian focus measure as described in Equation 4, we found that we could reliably distinguish a clear maximal focus value when performing sweeps, an example is shown in Figure 4. Applying Variance of Laplacian as a focus measure for our autofocus algorithm with the 2.0-magnification lens, we consistently find an optimal focus position, with standard deviation $\bar{\sigma} = 0.107mm$. As such, we find optimal focus with a 95%-confidence interval of $\pm 214\mu m$, compared to a depth of field of $\pm 200\mu m$.

DEPTH FROM DEFOCUS

In our current autofocus algorithm we compute the focus measure for an entire frame at a time, which under the assumption that the focal and the build plane are perfectly aligned, would be a completely fine approach. However, this is a naive assumption since the building plate and vat are manually mounted prior to each print, due to cleaning and object extraction. This is implausible to accomplish with micrometer precision consistently. To take this non-alignedness into account, we have constructed a depth map of of the build plane using depth from defocus [7], [8]. Our depth from defocus implementation is illustrated in Figure 6. Consider a camera with resolution of $N \times M$ which captures K images along the optical axis, each with a displacement of Δd . The kernel based focus measure FM is evaluated at a position (i, j) for all images. As such, this yields a stack of K focus measure evaluations, F .

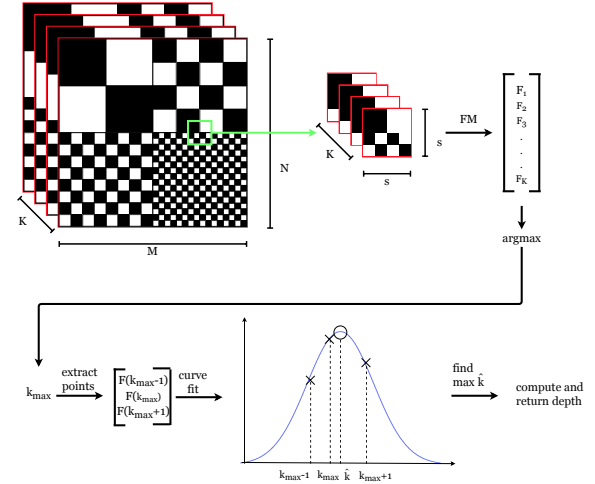


Figure 6: An illustration of computing Depth from Defocus for a single pixel-stack. K is the number of images in our stack, $M \times N$ is the size of our images, s is the kernel-size for our focus measure FM . \hat{k} is the estimated depth in of the pixel in question.

Now, we find the position of maximum focus

$$k_{max} = \arg \max_{k \in K} F_k, \quad (8)$$

and a Gaussian function G is interpolated using $F^{k_{max}-1}, F^{k_{max}}, F^{k_{max}+1}$. The top point \hat{k} of the interpolating Gaussian function is found and this is the estimated point of optimal focus for the pixel stack at (i, j) . Computing this for all pixel stacks yields a position map $\hat{k}(i, j)$ for the entire object. The actual depth of each position \hat{k} can then simply be computed from Δd and the initial distance between the camera and the object to create a depth map $D(i, j)$. The depth map of the printing plane computed using depth from defocus is illustrated in Figure 7.

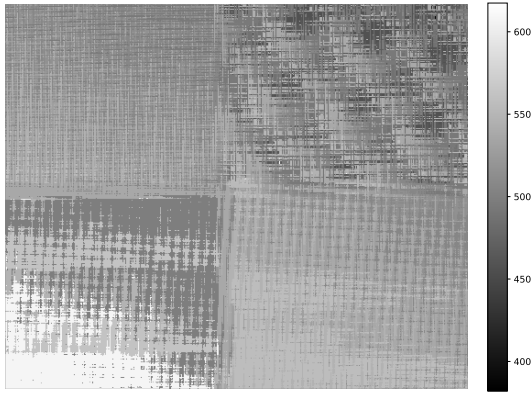


Figure 7: Depth map of the printing plane. $[0, 750]$ corresponds to $[322.000mm, 323.500mm]$, stepsize of $0.002mm$, kernel size of 25, image downsampled by factor 4.

While the depth map in Figure 7 clearly contains inaccuracies due to the quartered nature of our projection pattern, there is a definite trend in the bottom left corner. There is clear indication that the bottom left corner is in focus at a lower height than the rest of the plane.

DISCUSSION

We find that when the algorithm is initialized with parameters that do not allow for the initial sweep to capture any information around the peak, the algorithm becomes highly unstable. The 95%-confidence interval found when experimenting with deliberately challenging initial parameters is two orders of magnitude larger than the depth of field ($\pm 0.2mm$) for the 2.0 magnification lens, illustrating that an initialization of parameters requires either some prior knowledge of the general location of the point of maximum focus, or simply a sufficiently fine initial step size.

When the initial parameters are chosen deliberately, the algorithm shows remarkable stability in finding an appropriate maximal focus. The 95%-confidence interval for the results with sensible parameters is just $\pm 0.214mm$ - just a few micrometers wider than the depth of field.

A central assumption in this project, is that the focal plane is aligned with the building plane. With depth from defocus we have proved that it is in fact possible to check this assumption with our implementation. From the depth map in Figure 7 it can be seen that the height difference between the bottom left and top right corner is approximately $0.25mm$, however this is under the general assumption that the projector projects light with an uniform intensity. Since all focus measures considered in this work are intensity based, unexpected changes in intensity leads to changes in focus evaluation. For global focus evaluations in our autofocus solution, small nonuniformities will not effect the overall focus measure much. In local

focus measures, as used in depth from defocus, this nonuniformity may have large effects on estimated depth. As shown in [9], the projected light is indeed nonuniform. As such, the depth estimated by depth of focus may very well stem from the nonuniformity of the pattern and not from the build plane and focal plane not being parallel.

CONCLUSION

Under acceptable initial conditions we have succeeded in automating the tedious task of manually adjusting the focus on the DTU MPPS presented in [1] and sketched out a general solution that should be possible to implement on most experimental MPPSs. The autofocus solution consistently finds an optimal focus in a range of $\pm 214\mu m$ for the 2.0-magnification lens, thus almost identical to the depth of focus of $\pm 200\mu m$, but with room for improvements. However, the estimated focus makes a good basis for the user to fine tune the focus manually in order to assure perfect focus. Hence the algorithm is not yet completely automated but we have shown that it is certainly possible to automate the task and we are working towards a fully automated solution. Our autofocus solution works under the assumption that the building plane is perfectly aligned with the focal plane. In order to check that assumption we have successfully shown a method, based on our focus studies, to estimate a depth map. This depth map can be used as a guide to align the projector with the building plane. In the long run, the goal is to integrate this depth estimation with our autofocus solution such that it automatically runs and calibrates the focus before starting each build cycle.

References

- [1] F. W. Andersen, "Optimization of an experimental DLP platform by construction and process studies," Technical University of Denmark, DTU Mechanical Engineering, 2018.
- [2] Visitech, "Specification and Data Sheet Projection Lens LRS-10 P/N 6501980,"
- [3] —, "Specification and Data Sheet Projection Lens LRS-20 P / N 6501990,"
- [4] S. Pertuz, D. Puig, and M. A. Garcia, "Analysis of focus measure operators for shape-from-focus," *Pattern Recognition*, vol. 46, no. 5, pp. 1415–1432, 2013, ISSN: 00313203. DOI: 10.1016/j.patcog.2012.11.011.
- [5] G. H. Zong, M. L. Sun, S. S. Bi, and D. Dong, "Research on wavelet based autofocus evaluation in micro-vision," *Chinese Journal of Aeronautics*, vol. 19, no. 3, pp. 239–246, 2006, ISSN: 10009361. DOI: 10.1016/S1000-9361(11)60351-8. [Online]. Available: [http://dx.doi.org/10.1016/S1000-9361\(11\)60351-8](http://dx.doi.org/10.1016/S1000-9361(11)60351-8).

- [6] S. Liu, M. Liu, and Z. Yang, "An image auto-focusing algorithm for industrial image measurement," *EURASIP Journal on Advances in Signal Processing*, 2016, ISSN: 1687-6180. DOI: 10.1186/s13634-016-0368-5. [Online]. Available: <http://dx.doi.org/10.1186/s13634-016-0368-5>.
- [7] S. N. Nayar, "Shape from Focus, Pattern Analysis and Machine Intelligence," *IEEE Transactions*, vol. 16, no. 8, pp. 824–831, 1994.
- [8] M. Moeller, M. Benning, C. Schönlieb, and D. Cremers, "Variational Depth from Focus Reconstruction," *IEEE Transactions on Image Processing*, vol. 24, no. 12, pp. 5369–5378, 2015, ISSN: 10577149. DOI: 10.1109/TIP.2015.2479469. arXiv: 1408.0173.
- [9] F. Warburg, M. M. Ribo, and D. B. Pedersen, "Intensity Mapping for Mask Projection based Photopolymerization," in *Advancing Precision in Additive Manufacturing*, 2018.